Progress In Electromagnetics Research B, Vol. 41, 187–211, 2012

ANALYSIS OF COUPLED MICROSTRIP LINES FOR QUAD-BAND EQUAL POWER DIVIDERS/COMBINERS

A. M. El-Tager[1, *], A. M. El-Akhdar[2], and H. M. El-Hennawy[2]

[1]Electronic Engineering Department, M.T.C., Cairo, Egypt

[2]Electronics and Communications Department, Ain Shams University, Cairo, Egypt

Abstract—This paper presents a novel quad-band power divider with equal power division ratio. The proposed power divider is realized using two cascaded sections of dual-band transformers based on coupled microstrip lines. Limitations of using dual-band quarter-wavelength transformers based on coupled lines are studied through parametric analysis to obtain useful design guidelines related to available fabrication facilities. General closed-form expressions are deduced to calculate design parameters. To verify analysis and design methodologies, a prototype of quad-band equal power divider is proposed. Compared to conventional quad-band power dividers using sections of transmission line transformers, the proposed power divider records a size reduction of about 20% and reduced parasitic effects at higher frequencies according to the usage of only two resistors instead of four with much smaller ohmic values. In addition, a quad-band power divider is proposed, fabricated and measured for 3G and 4G applications at 2.1, 2.5, 3.5, and 3.8 GHz frequencies. Measured and simulated data are in very good agreement which validates the novel design.

1. INTRODUCTION

Microstrip power dividers/combiners are widely used in RF/microwave front-end systems such as power amplifiers, mixers, feed network of an antenna array system for distribution of low-power signals and laboratory equipments. Many studies are made for device miniaturization [1–5], Ultra-wide band [6–8], and multiband operation [9–11]. They have

Received 8 March 2012, Accepted 21 May 2012, Scheduled 4 June 2012

* Corresponding author: Ayman Mohamed Elsaye El-Tager (aeltager@yahoo.ca).

been subject of interest in recent years within the microwave engineering community.

Modern wireless communication systems operate in dual-band and multi-band frequencies. Therefore, many researchers developed dual-band RF components such as antennas [12] and power dividers/combiners [13–16]. Power dividers and combiners play an essential role in microwave and millimetric wave systems. Several dual-band Wilkinson power dividers have been developed based on Monzon's dual-band transformer using two cascaded sections of transmission line transformers [17]. His theory was extended to provide tri-band [18] and quad-band [19] transformers using cascaded transmission lines, which are further more used in the design of multi-band power dividers/combiners [20–22]. Dual-band power dividers can also be achieved using T-sections [23] and Pi structures [24–26] by connecting open or short stubs to the conventional transmission line, but the main drawback of using such techniques is their large physical size. Another modification technique could be presented to provide dual-band power dividers using artificial planar transmission lines [27–29], which need a very high resolution facility in fabrication.

On the other hand, dual-band power dividers can be achieved using four cascaded sections of $1/6$ wavelength transmission lines with different characteristic impedances of transmission line transformers [30], as shown in Figure 1, which is limited to a frequency and its first harmonic. To get rid of this limitation, a modification is done by connecting series or parallel RLC circuits instead of the isolation resistor, according to any desired frequency ratio [31], but this is limited to low frequency applications. Another modification is applied by connecting two open stubs between the cascaded sections of transmission lines [32], as illustrated in Figure 2 which suffers a larger physical size. A third modification is presented by replacing the conventional quarter wave transmission line with a π-section [33] as shown in Figure 3. Finally, a dual-band transformer based on coupled microstrip lines is presented in [34], as shown in Figure 4. This technique has many advantages; first: size reduction over the presented techniques in Figure 2 and Figure 3, second: there is no need to use any reactive components as in Figure 1. Therefore, this technique will be adopted throughout this

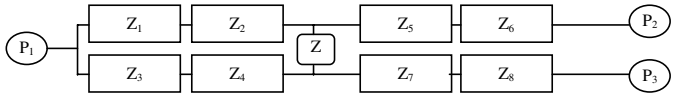

Figure 1. Dual-band power divider using cascaded $\lambda/6$ sections [30, 31].

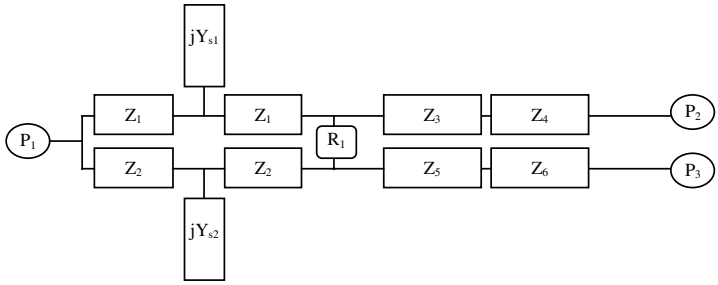

Figure 2. Dual-band power divider using T-sections [32].

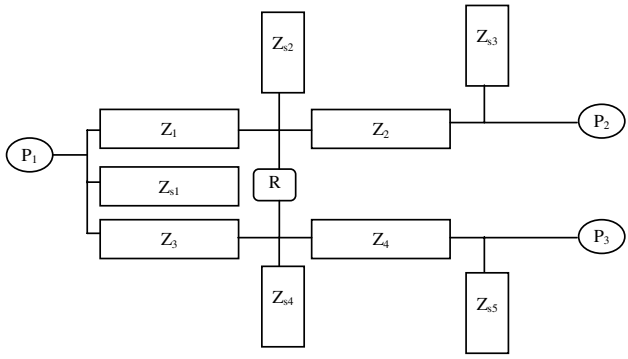

Figure 3. Dual-band power divider using π-sections [33].

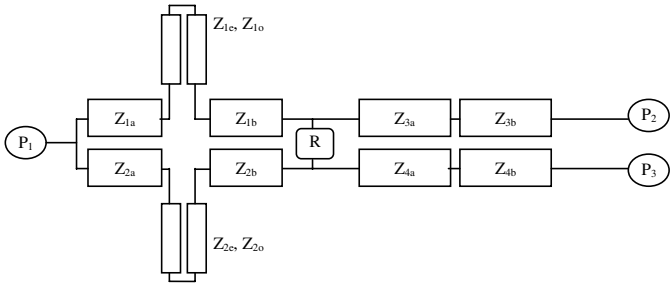

Figure 4. Dual-band power divider based on coupled lines [34].

work. But it has some limitations, such as frequency ratio constraints while realizing feasible coupled microstrip lines. This will be studied throughout this paper to obtain some guidelines for other designers. Furthermore, a closed form expression is introduced to calculate design parameters.

In this paper, the technique of dual-band transformers based on coupled microstrip lines is studied. Some parametric analyses are obtained through normalized curves to highlight the advantages as well as the limitations of this technique. Then, a general closed-form expression to calculate the design parameters is deduced. Furthermore, this technique is employed to propose a novel quad-band power divider with equal power split. The idea of this proposal is based on replacing each single-band transmission line transformer used in conventional dual-band Wilkinson power dividers [20] by its equivalent dual-band structure based on coupled microstrip lines studied in this paper. In other words; Monzon's theory is extended to be realized using coupled microstrip lines with realistic impedance values for the sake of achieving reduced size quad-band power dividers with flexible layout design. This paper is organized in six Sections. Section 2 introduces general expressions as well as parametric analyses used to calculate the design parameters of dual-band transformers based on coupled lines. In Section 3, analysis of the quad-band power divider and the combination of both techniques are proposed. Section 4 shows the design, fabrication and measurements of the proposed prototype. Section 5 compares the proposed technique to other published two-way quad-band power dividers/combiners. Finally, Section 6 presents the conclusions of this work.

2. STUDY OF DUAL BAND TRANSFORMER USING COUPLED MICROSTRIP LINES

Many studies were made to convert the conventional single band transmission lines to operate as dual-band ones. This section presents dual-band transformers based on coupled microstrip lines illustrated in Figure 5(a). Such transformers are of great interest because of the current trend toward compact, more efficient, dual-band RF front ends. This section also presents the generalization of the closed form expressions used in the design of dual-band transformer based on coupled microstrip lines. In addition, some design guidelines are proposed throughout further parametric analysis.

Dual-band transformer based on coupled microstrip lines shown in Figure 5(a) consists of two branch transmission lines with characteristic impedances Z_m and coupled microstrip lines connected between the two branch lines having characteristic impedances of Z_{ne} and Z_{no}. Characteristic impedances are tuned to the average frequency $f_o = (f_1 + f_2)/2$; where f_1 is the center frequency of the first operating band and f_2 is the center frequency of the second operating band. θ_i represents the electrical length of dual-band transformer either at

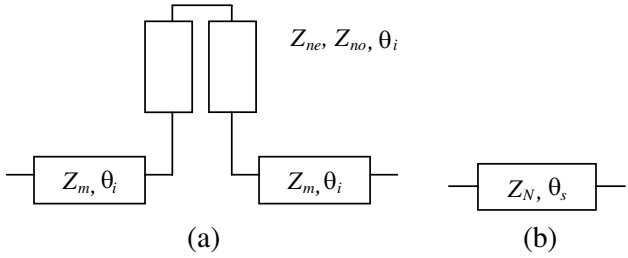

Figure 5. (a) Dual-band transformer based on coupled lines and (b) its equivalent single-band transformer circuit.

frequency f_1 which will be θ_1 or at frequency f_2 which will be θ_2. On the other hand, Figure 5(b) shows the equivalent single-band transmission line transformer having characteristic impedance Z_N and electrical length θ_s.

2.1. Theory and Analysis

In this section; the general expressions used to design dual-band transformer based on coupled lines is presented. Analysis will take place by comparing dual-band transformer based on coupled lines with its equivalent circuit of single-band transformer. This is known as replacing single-band elements with dual-band elements technique. As shown in Figure 5, main design parameters are:

(i) Single-band transformer characteristic impedance (Z_N).
(ii) Single-band transformer electrical length (θ_s).
(iii) Dual-band transformer branch lines characteristic impedances (Z_m).
(iv) Frequency ratio of the dual-band transformer (f_2/f_1).

Due to the symmetric property of the dual frequency transformer the even-odd decomposition method is used to obtain a general expression for calculating design parameters. Where

$$\theta_o = \frac{\theta_1 + \theta_2}{2} = \theta_s \tag{1}$$

$$f_o = \frac{f_1 + f_2}{2} \tag{2}$$

Even or odd half circuit design parameters are calculated using transmission line theory as follows:

2.1.1. Even Mode Analysis

From the transmission line theory, all ports look open for even mode analysis. According to Figure 6(a)

$$Z_{in}^{e} = jZ_m \frac{-Z_{ne}+Z_m \cdot \tan^2\theta_i}{(Z_m + Z_{ne}) \cdot \tan\theta_i} \tag{3}$$

While from Figure 6(b)

$$Z_{in}^{e} = -jZ_N \cdot \cot\left(\frac{\theta_s}{2}\right) \tag{4}$$

By equating Equations (3) and (4) we get:

$$Z_N = Z_m \frac{Z_{ne}-Z_m \cdot \tan^2\theta_i}{(Z_m + Z_{ne}) \cdot \tan\theta_i \cdot \cot\left(\frac{\theta_s}{2}\right)} \tag{5}$$

Or,

$$Z_{ne} = Z_m \frac{Z_m \cdot \tan^2\theta_i - Z_N \cdot \cot\left(\frac{\theta_s}{2}\right) \cdot \tan\theta_i}{Z_m + Z_N \cdot \cot\left(\frac{\theta_s}{2}\right) \cdot \tan\theta_i} \tag{6}$$

2.1.2. Odd Mode Analysis

From transmission line theory, all ports are shorted for odd mode analysis. From Figure 7(a)

$$Z_{in}^{o} = jZ_m \frac{\tan\theta_i \cdot (Z_{no} + Z_m)}{Z_m - Z_{no} \cdot \tan^2\theta_i} \tag{7}$$

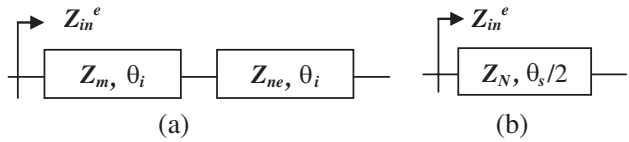

Figure 6. (a) Even mode half circuit, (b) its equivalent circuit.

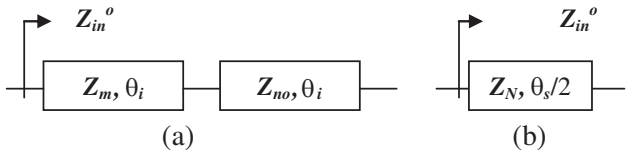

Figure 7. (a) Odd mode half circuit, (b) its equivalent circuit.

And from Figure 7(b)

$$Z_{in}^{o} = jZ_N \cdot \tan\left(\frac{\theta_s}{2}\right) \tag{8}$$

From Equations (7) and (8) we get

$$Z_N = Z_m \frac{(Z_{no} + Z_m) \cdot \tan\theta_i \cdot \tan\left(\frac{\theta_s}{2}\right)}{Z_m - Z_{no} \cdot \tan^2\theta_i} \tag{9}$$

Or

$$Z_{no} = Z_m \frac{Z_N \cdot \tan\left(\frac{\theta_s}{2}\right) + Z_m \cdot \tan\theta_i}{Z_N \cdot \tan\left(\frac{\theta_s}{2}\right) \cdot \tan^2\theta_i - Z_m \cdot \tan\theta_i} \tag{10}$$

2.1.3. General Expressions

Now after calculating the characteristic impedances of the coupled lines, an expression for the electrical length of the dual-band transformer is to be obtained.

By definition we have,

$$\frac{\theta_2}{\theta_1} = \frac{f_2}{f_1} \tag{11}$$

From Equation (1) we have

$$\theta_1 = 2\theta_s - \theta_2 \tag{12}$$

Substituting Equation (12) in Equation (13) leads to

$$\theta_1 = \theta_s \cdot \left(\frac{f_1}{f_o}\right) \tag{13}$$

And similarly

$$\theta_2 = \theta_s \cdot \left(\frac{f_2}{f_o}\right) \tag{14}$$

From Equations (13) or (14), Equations (6) and (10) can be rewritten as

$$Z_{ne} = Z_m \frac{Z_m \cdot \tan^2\left[\theta_s \cdot \left(\frac{f_1}{f_o}\right)\right] - Z_N \cdot \cot\left(\frac{\theta_s}{2}\right) \cdot \tan\left[\theta_s \cdot \left(\frac{f_1}{f_o}\right)\right]}{Z_m + Z_N \cdot \cot\left(\frac{\theta_s}{2}\right) \cdot \tan\left[\theta_s \cdot \left(\frac{f_1}{f_o}\right)\right]} \tag{15}$$

And

$$Z_{no} = Z_m \frac{Z_N \cdot \tan\left(\frac{\theta_s}{2}\right) + Z_m \cdot \tan\left[\theta_s \cdot \left(\frac{f_1}{f_o}\right)\right]}{Z_N \cdot \tan\left(\frac{\theta_s}{2}\right) \cdot \tan^2\left[\theta_s \cdot \left(\frac{f_1}{f_o}\right)\right] - Z_m \cdot \tan\left[\theta_s \cdot \left(\frac{f_1}{f_o}\right)\right]} \tag{16}$$

Equations (15) and (16) are considered as general expressions containing all design variables of the dual-band transformer based on coupled microstrip lines, which are; Z_N, θ_s, (f_2/f_1) and Z_m. This section studies the relations between the design variables and how they could affect the choice of coupled lines characteristic impedances Z_{ne} and Z_{no} which may lead to a non-realizable solution if miss chosen. Therefore, to provide design guide, a closed form expression is introduced in Appendix A to choose Z_m. Moreover, further parametric analyzes are studied in the next section to choose Z_m graphically for certain required frequency ratio with realizable values of coupled microstrip lines.

2.2. Parametric Analysis

Usually, Z_N is given, while for quarter wave length transformers, θ_s is chosen to be 90 degrees. But the frequency ratio (f_2/f_1) needs more investigation. Based on the analysis introduced in [34], it should be less than 1.64. By further insight thinking about this limit it is found to be non-realizable and requires more determination. In order to determine the limitation and to obtain a degree of freedom in realizing the coupled microstrip lines, a new coefficient q' is introduced. Assuming q' is the difference between Z_{ne} and Z_{no}. While, a variable q is defined as q' normalized to Z_o which is the geometric mean of Z_{ne} and $Z_{no}(Z_o = (Z_{ev} \cdot Z_{od})^{1/2})$ [35, 36]. It is called a realization coefficient, which helps designers to obtain a feasible realizable solution as shown in this section.

$$q = \frac{q'}{Z_o} \tag{17}$$

$$q' - qZ_o = 0 \tag{17a}$$

where

$$q' = Z_{ne} - Z_{no} \tag{17b}$$

$$Z_o = \sqrt{Z_{ne}Z_{no}} \tag{17c}$$

2.2.1. Variation of Frequency Ratio F_r

Figure 8(a) shows the coupled lines characteristic impedances at different values of Z_m. Figure 8(a) shows the curves presented in Figure 6 of Ref. [34] at different values of Z_m. While Figure 8(b) shows how the introduced realization coefficient (q) is varying versus the frequency ratio at different values of branch line characteristic

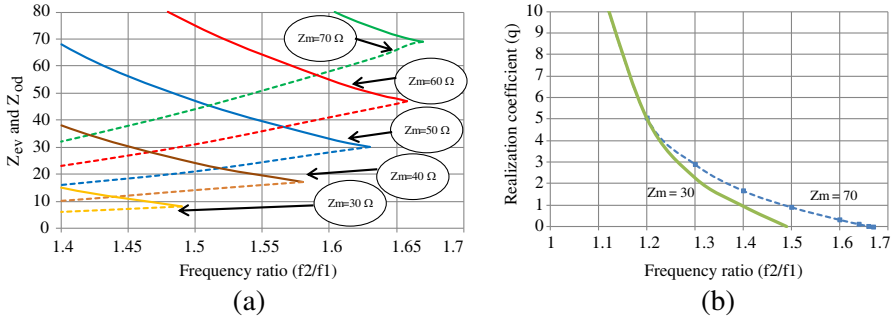

Figure 8. (a) Coupled lines characteristic impedances (Z_{ev} and Z_{od}), (b) realization coefficient q versus frequency ratio F_r at different values of Z_m.

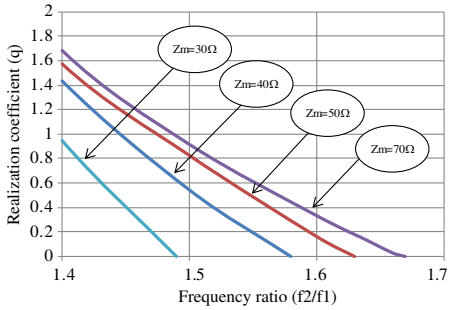

Figure 9. Realization coefficient versus frequency ratio at different values of Z_m.

impedance Z_m. In Figure 8(b), the solid line presents the curve of $Z_m = 30\,\Omega$. While, the dashed line shows the curve of $Z_m = 70\,\Omega$.

From Figure 8, it is observed that as frequency ratio increases, Z_m increases (but it shouldn't exceed the value of Z_N, otherwise it will lead to unacceptable solution). Although this curve plots q with large values, for feasible realization of coupled microstrip lines, the realization coefficient q is usually small (may be less than 2) as shown in Figure 9, because as q decreases F_r increases. On the other hand, Figure 9 can be used to determine the maximum allowed q at certain Z_m and certain F_r. Therefore, further investigation of this realization coefficient is presented as follows.

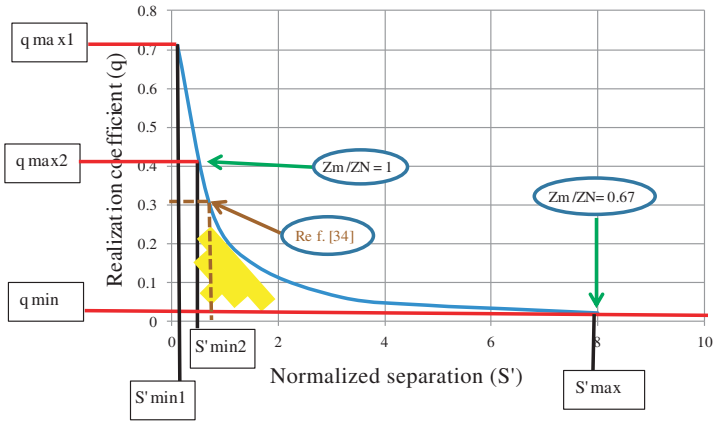

Figure 10. Realization coefficient (q) versus separation between coupled lines (S').

2.2.2. Separation between Coupled Lines

Figure 10 introduces the relation between coupled lines characteristic impedances (Z_{ev} and Z_{od}) presented in the realization coefficient (q) and the separation between coupled lines with respect to substrate thickness ($S' = S/H$). This normalized curve is important to realize feasible dual-band transformer based on coupled microstrip lines. Usually, the available fabrication process has certain resolution which limits (S') to a certain minimum value $S'_{\min}$ which determines $q_{\max 1}$. On the other hand, the maximum separation limit $S'_{\max}$ which corresponds to $q_{\min}$ is determined by the condition ($Z_{ev} = Z_{od}$) at which ($Z_m/Z_N = 0.67$). One can observe that the region of normalized separation is ($S'_{\min} < S/H < 8$), which is different from that of conventional coupled lines ($0.1 < S/H < 10$). However, for more practically realizable dual-band transformer based on coupled microstrip lines, a region of solution is provided starting from ($Z_N = Z_m$) which is $q_{\max 2}$, that dominates the maximum limit of q. Therefore, the minimum frequency ratio F_r is to be obtained applying the maximum q from Figure 10 into Figure 9. It is clear from Figure 10 that the realization coefficient q can vary in ($0.04 < q < 0.72$), while the design example of reference [34] is plotted, giving $q = 0.32$.

2.2.3. Choice of Z_m

Figure 11 shows the variation of realization coefficient (q) versus the normalized branch line characteristic impedance Z_m at different

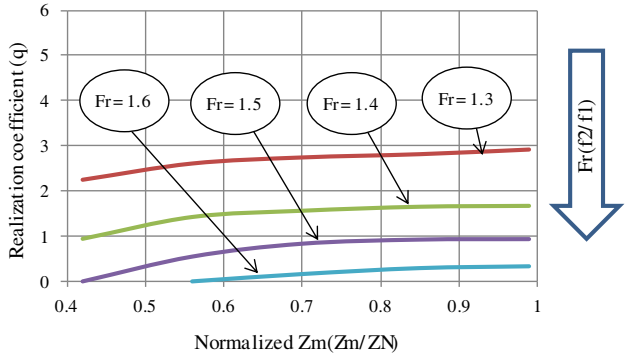

Figure 11. Realization coefficient (q) versus normalized branch impedance Z_m at different frequency ratios F_r.

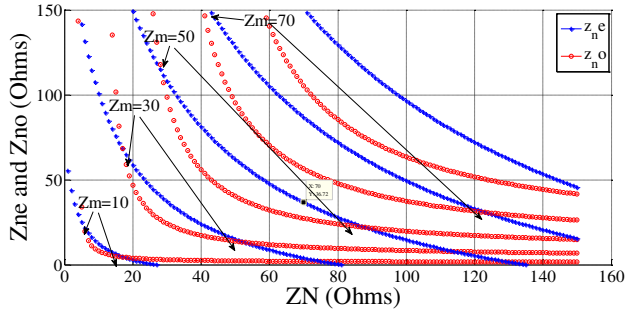

Figure 12. Variation of Z_{ne} and Z_{no} with Z_N at different values of Z_m.

frequency ratios (F_r). It is recognized that the realization coefficient (q) increases, as the frequency ratio decreases. On the other hand, for certain frequency ratio, as Z_m increases, the realization coefficient (q) slightly increases. This observation is matched with the results obtained in Figure 9. If the designer needs higher frequency ratio, Z_m should be chosen with higher value. But, the maximum allowed Z_m is limited by the value of Z_N to satisfy ($Z_m/Z_N = 1$).

Moreover, Z_m can also be determined graphically through Figure 12. It shows the relation between single band characteristic impedance Z_N and coupled lines characteristic impedances Z_{ne} and Z_{no} at different values of branch lines characteristic impedances Z_m. Figure 12 shows the acceptable and unacceptable solutions of Z_m. For example if we pick $Z_m = 30\,\Omega$, that leads to unacceptable solution because $Z_{no} > Z_{ne}$. On the other hand, if we choose $Z_m = 70\,\Omega$,

that will lead to an acceptable solution but with large value of q' that yields to small separation between microstrip coupled lines through realization. Based on certain microstrip fabrication process this small separation might not be realizable. For simplicity an expression to calculate the optimum value of branch line characteristic impedance Z_m is introduced in Appendix A.

From the previous studies, we can define the unacceptable region of solutions in the following conditions:

a) $Z_{ne} < Z_{no}$, which is unacceptable solution.
b) $q' > Z_o$, that obtains tight separation between coupled lines which might not be reached in the available fabrication process.
c) If the difference q' is very small, a large separation between coupled microstrip lines occurs leading to extra radiation losses.

As a conclusion, this section presented the variation of design parameters and how they affect the coupled lines characteristic impedances using both analytical and graphical solutions. The following section presents the application of these dual-band coupled lines to design a novel quad-band power divider with equal power split.

3. DESIGN OF PROPOSED QUAD-BAND POWER DIVIDER

This section proposes a novel design methodology of quad-band power divider/combiner with equal power division ratio. The proposed power divider consists of two sections of dual-band transformers based on coupled microstrip lines. Each single-band transmission line transformer used in dual-band Wilkinson power divider shown in Figure 13 is replaced by its equivalent dual-band structure based on the previously studied coupled microstrip lines technique.

Figure 13 presents dual-band Wilkinson power divider. The power divider consists of two sections of transmission line transformers and two isolation resistors for port isolation. This conventional technique

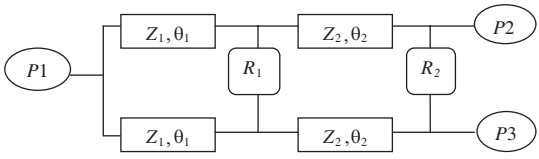

Figure 13. Dual-band Wilkinson power divider based on Monzon's theory for cascaded transmission line transformers [20].

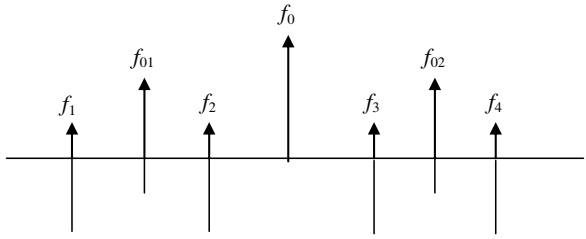

Figure 14. Frequency line indicator.

is utilized to provide tri-band (using three sections of transmission line transformers) [21] and quad-band (using four sections of transmission line transformer) [22]. The former conventional technique is to be compared to the novel design of this work in Section 5. The proposed design methodology is presented as follows:

1) Starting with a given four frequencies f_1, f_2, f_3, and f_4, and exploiting the symmetric property of the dual-band transformer as shown in Figure 14, the intermediate frequencies f_{o1} and f_{o2} are calculated using Equations (18) and (19) as follows:

$$f_{01} = \frac{f_1 + f_2}{2} \tag{18}$$

$$f_{02} = \frac{f_3 + f_4}{2} \tag{19}$$

While, the center frequency f_o is calculated using Equation (20) as follows:

$$f_0 = \frac{f_{o1} + f_{o2}}{2} \tag{20}$$

2) The design parameters Z_1 and Z_2 in the conventional Wilkinson power divider shown in Figure 13 are calculated using Monzon's expression shown in Equations (21) and (22)

$$Z_2 = Z_o \sqrt{\frac{1}{2\alpha} + \sqrt{\frac{1}{4\alpha^2} + 2}} \tag{21}$$

$$Z_1 = \frac{2Z_o^2}{Z_2} \tag{22}$$

where;

$$\alpha = \tan^2(\beta l) = P^2 \quad \text{and} \quad P = \frac{n\pi}{1+m}$$

m presents the frequency ratio (f_2/f_1).

3) The isolation resistors R_1 and R_2 are calculated using Equations (23) and (24) as follows:

$$R_1 = \sqrt{\frac{BE}{AD}} \tag{23}$$

$$R_2 = \frac{E}{C - DR_1} \tag{24}$$

where

$$A = 2Z_2\left(1 + \frac{Z_2T_2}{Z_1T_1}\right) \tag{a}$$

$$B = 2Z_2 \tag{b}$$

$$C = \frac{2Z_2^2T_2}{Z_o} \tag{c}$$

$$D = \left(T_2 - \frac{Z_2}{Z_1T_1}\right) \tag{d}$$

$$E = 2Z_oC \tag{e}$$

$$T_1 = \tan B_1l_1 \tag{f}$$

$$T_2 = \tan B_2l_2 \tag{g}$$

Next step is to replace each single band transmission line by its equivalent dual-band structure based on coupled microstrip lines as shown in Figure 15. The design procedure of this step is obtained graphically suing parametric analysis of Section 2.2 and analytically using Equations (15), (16), (17) and Appendix A.

As a conclusion, this section presented the design guidelines to provide quad-band power divider using two cascaded sections of dual-band transformers based on coupled microstrip lines. This design

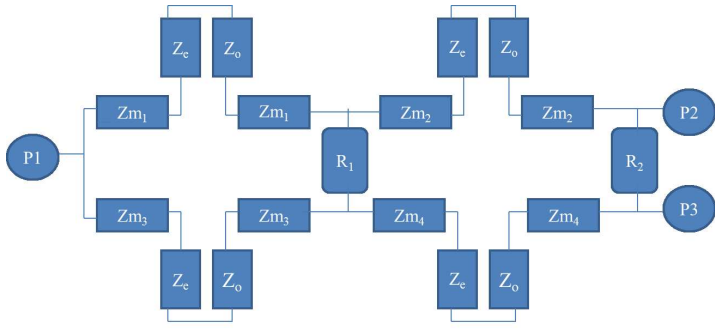

Figure 15. Novel quad-band power divider based on coupled microstrip lines.

procedure is summarized in the flowchart of Appendix B. Section 4 verifies this design methodology through a fabricated prototype. On the other hand, Section 5 compares this novel technique to conventional quad-band power divider techniques.

4. PROPOSED QUAD-BAND POWER DIVIDER FOR 3G AND 4G APPLICATIONS

This section presents design, fabrication and measurements of a quad-band power divider with equal power division based on coupled microstrip lines. The proposed power divider is useful for 3G and 4G, such as WiMax and UMTS applications. It operates at frequencies 2.1 GHz, 2.5 GHz, 3.5 GHz, and 3.8 GHz. It is interesting to mention that the proposed design satisfies 3G and 4G application bandwidths.

4.1. Realization Using Coupled Microstrip Lines

Following the design process proposed in the flowchart of Appendix B, a quad-band power divider with equal power division is designed as follows:

- Using Equations (19) and (20) we obtain $Z_N = Z_{N1} = Z_{N2} = 70.7\,\Omega$ for $\theta_s = \theta_{s1} = \theta_{s2} = \theta_{s3} = \theta_{s4} = 90$ degrees.
- Graphically, using Figures 8 through 12 or analytically, using the deduced expression of Appendix A, the branch line characteristic impedance can be calculated as follows:
  - Using the general expression from Equations (15), (16), and the closed form expression presented. The branch lines characteristic impedance Z_m is calculated using the closed form expression presented in Appendix A, and graphically using the design curves presented in Figures 10 through 12 as follows:
    - $Z_m = Z_{m1} = Z_{m2} = Z_{m3} = Z_{m4} = 50\,\Omega$
    - $Z_e = Z_{e1} = Z_{e2} = Z_{e3} = Z_{e4} = 36\,\Omega$
    - $Z_o = Z_{o1} = Z_{o2} = Z_{o3} = Z_{o4} = 27\,\Omega$
- The isolation resistors R_1 and R_2 are calculated using Equations (23) and (24).

After calculating the design parameters of the quad-band power divider, quad-band power divider is realized as shown in Figure 15 using low loss Teflon substrate RT/Duroid6010 with relative dielectric constant $\varepsilon_r = 10.5$, height $H = 50$ mil, metal thickness $T = 17\,\mu$m, and loss tangent $\tan\delta = 0.001$. Table 1 presents the final realized physical parameters of the proposed microstrip transformer.

Table 1. Physical parameters of the proposed quad-band power divider.

Parameters	Coupled lines			Branch lines		Isolation resistor Ω	
Electrical parameters	$Z_{1e} = Z_{2e} = Z_{3e} = Z_{4e}$		$Z_{1o} = Z_{2o} = Z_{3o} = Z_{4o}$	$Z_{m1} = Z_{m2} = Z_{m3} = Z_{m4}$		R_1	R_2
Impedances (Ω)	36		27	50		100	200
Physical values (mm)	Width	Separation	Length	Width	Length	100	200
	2.4	0.75	9.12	1.1	9.5		

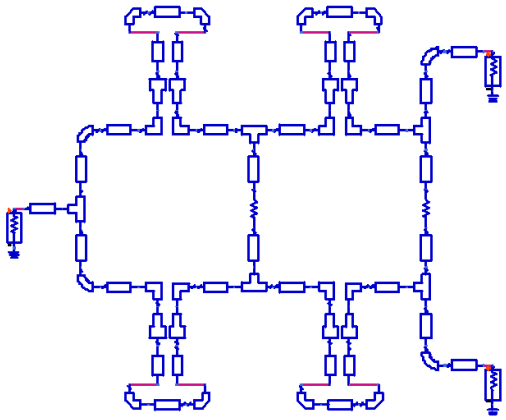

Figure 16. Schematic of the proposed quad-band equal power divider.

4.2. Design Simulations and Layout Generation

This section presents the simulation of the proposed quad-band power divider based on coupled microstrip lines to include all microstrip discontinuities and to prepare the design for layout generation process. Figure 16 shows the schematic of quad-band equal power divider. The simulation is done using Agilent ADS. Resultant Scattering parameters of the proposed structure are plotted when compared to measured parameters in Section 4.3.

4.3. Fabrication and Measurements

The designed proposed prototype is fabricated, which gives promising measurements. Figure 17 shows the fabricated prototype of the proposed quad-band equal power divider based on coupled microstrip

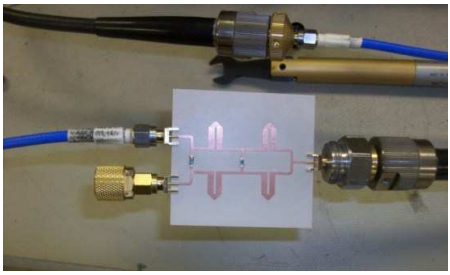

Figure 17. Quad-band power divider connected to the HP8510c VNA.

Table 2. Measured S-parameters of quad-band power divider.

Parameters	2.1 GHz	2.5 GHz	3.5 GHz	3.8 GHz	Notes
Input return loss	15	13	11	15	> 11 dB
Output return loss	21	15	15	22	> 15 dB
Insertion loss	0.05	0.4	0.6	0.6	< 0.6 dB
Isolation between P1 & P2	21	26	15	15	> 15 dB

lines. The proposed quad-band equal power divider based on coupled microstrip lines has a physical size of 5.5 cm × 3 cm. Figure 18 shows the simulated and measured return losses $|S_{11}|$, $|S_{22}|$ and $|S_{33}|$ of the designed quad-band power divider. While Figure 19 presents the measured insertion $|S_{12}|$, $|S_{13}|$ and isolation $|S_{23}|$.

Figure 18 shows that measured input return loss $|S_{11}|$ is better than 11 dB, while output return losses $|S_{22}|$ and $|S_{33}|$ are better than 15 dB. Figure 19 shows that measured insertion losses $|S_{12}|$ and $|S_{13}|$ are better than 0.6 dB compared to ideal 3 dB level, while measured isolation is better than 15 dB at the four operating frequencies. The measured S-parameters are recorded in Table 2.

Measurement process is done using HP8510c VNA as shown in Figure 17. There are some slight discrepancies between measurements and simulations which may be due to any uncounted microstrip discontinuities and/or tolerances in the fabrication process. The quad-band equal power divider based on coupled microstrip lines records promising measurements at the four operating frequencies.

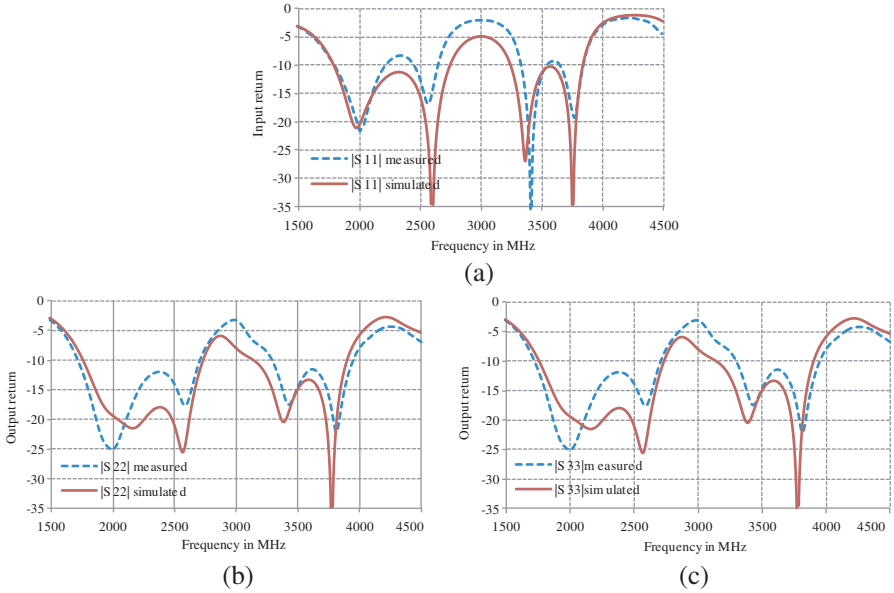

Figure 18. Simulated and measured return losses (a) Magnitude of $|S_{11}|$. (b) Magnitude of $|S_{22}|$. (c) Magnitude of $|S_{33}|$.

Next section presents a comparison between quad-band power divider using other techniques, and also presents the features of the provided design.

5. COMPARISON TO OTHER CONVENTIONAL TECHNIQUES

Figure 20 shows quad-band equal power split power divider using cascaded sections of transmission line transformers, and four resistors connected at the end of each section to provide matching and isolation presented in [22]. It operates at harmonic frequencies 0.5, 1, 1.5, and 2 GHz. The presented quad-band power divider based on cascaded sections of transmission line transformers has some disadvantages: 1) long physical length of the divider due to the usage of four cascaded sections of transmission line transformers which have been reduced by using curved transmission lines instead of the conventional straight ones as shown in Figure 21. 2) Parasitic effects caused by the four resistors. 3) The need of an optimization CAD tool (swarm particle optimization). 4) Applicable only for low frequency applications according to the high values of the used isolation resistors

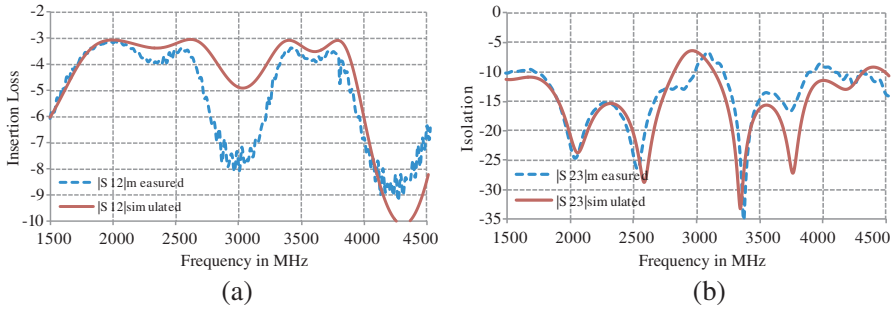

Figure 19. Measured and simulated (a) insertion $|S_{12}|$ and (b) isolation $|S_{23}|$.

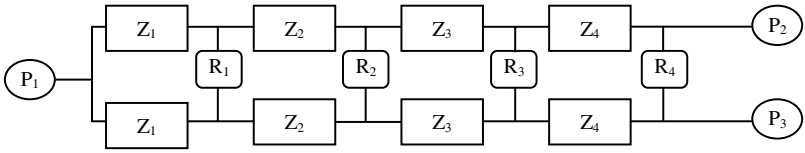

Figure 20. Quad-band power divider presented in [22].

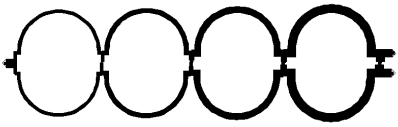

Figure 21. Quad-band power divider using cascaded sections of transmission line transformers as presented in [22].

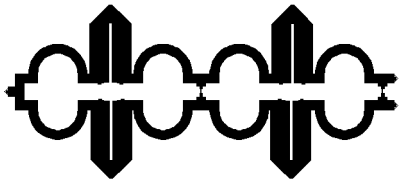

Figure 22. Quad-band equal power divider using curved transmission lines based on this work.

(maximum value is 400 Ω). On the other hand, a proposed quad-band equal power divider based on coupled microstrip lines based on this work and utilizing curved transmission lines is presented as shown in Figure 22. The proposed power divider based on coupled microstrip lines operates at frequencies 1.1, 1.4, 1.8, 2.1 GHz. Table 3 shows the comparison between the two quad-band power dividers. Quad-band power divider presented in this work illustrated in Figure 22 features reduced size, reduced parasitic effect, and simplicity in design parameters calculation.

Table 3. Comparison between quad-band equal power dividers.

Parameters	**This work**	**Ref. [22]**	**Enhancement [%]**	**Comments**
Need of Particle swarm optimization method	No	Yes	Analytical solution is presented	Simplicity in direct substitution
Size [cm × cm]	10×5	12×5	20 %	Length reduction
No. of Isolation Resistors	Only 2	4	50%	Less parasitic effects
Max. Resistor Value (Ω)	200	400	50%	Applicable for higher frequency applications

Table 3 shows a size reduction of about 20%. The presented design uses only two isolation resistors with reduced values, which allows operation in higher frequencies with reduced parasitic effects. The proposed design has a bit degraded performance compared to the one presented in [22] but, it fulfills the power dividers performance. The recorded input return loss is better than 14 dB at the four operating frequencies. Output return losses are better than 15 dB. The recorded insertion losses are better than 0.3 dB, while the recorded isolation between the output ports is better than 19 dB at the four design frequencies.

6. CONCLUSION

This paper presents a novel design of Quad-band power divider/combiner with equal power division ratio; the divider uses two cascaded sections of dual-band transformers based on coupled microstrip lines. Moreover, the used dual-band transformer based on coupled microstrip lines are studied and analysed to obtain a closed form expression for the determination of the design parameters. Further parametric analyses are conducted using general normalized curves to help designers to obtain a realizable solution based on their available fabrication process resolution. The proposed power divider features reduced size and uses fewer resistors with lower values than other con-

ventional techniques which make it applicable to higher frequencies. A proposed prototype is designed, simulated and fabricated at 2.1, 2.5, 3.5 and 3.8 GHz for 3G and 4G applications. The achieved agreement between simulations and measurements verifies the design methodology and make the proposed structure very promising. The proposed design could be easily tailored to be applied in package level such as Low temperature co-fired ceramics (LTCC) and chip level such as CMOS and GaAs Monolithic microwave integrated circuits (MMIC).

APPENDIX A.

The branch line characteristic impedance can be a design freedom. The following expression helps the designer to calculate the branch line impedance which will provide an optimum solution for the coupled lines characteristic impedances Z_{ev} and Z_{od}. For simplicity the design parameters used in the coupled lines characteristic impedances are stated as follows:

$$a = Z_m \tag{A1}$$

$$b = Z_N \tag{A2}$$

$$c = \tan\left[\theta_s \cdot \left(\frac{f_1}{f_o}\right)\right] \tag{A3}$$

$$d = \tan\left(\frac{\theta_s}{2}\right) \tag{A4}$$

The following expressions are used to calculate the branch line impedance Z_m:

$$Z_m = \frac{\alpha_1 + \sqrt{\beta}_1}{\delta_1} \tag{A5}$$

where

$$\alpha_1 = qd^2 + 2d^2 - 2d^2c^4 + qc^4d^2 + 2qc^2 \tag{A6}$$

$$\begin{aligned}\beta_1 = {} & 4d^4 + 2q^2d^4c^4 - 4d^4c^8q + 8d^2c^6q + q^2c^8d^4 \\ & -8qc^2d^2 + q^2d^4 + 4qd^4 - 8d^4c^4 + 4d^4c^8 + 4q^2c^2 \\ & -16c^6d^2 - 32d^2c^4 + 8q^2c^4d^2 - 16d^2c^2\end{aligned} \tag{A7}$$

$$\delta_1 = \frac{b}{2cd\left(-2c^2 - 2 + qc^2 - q\right)} \tag{A8}$$

APPENDIX B.

Proposed design steps used to calculate the design parameters of quad-band equal power divider based on coupled microstrip lines.

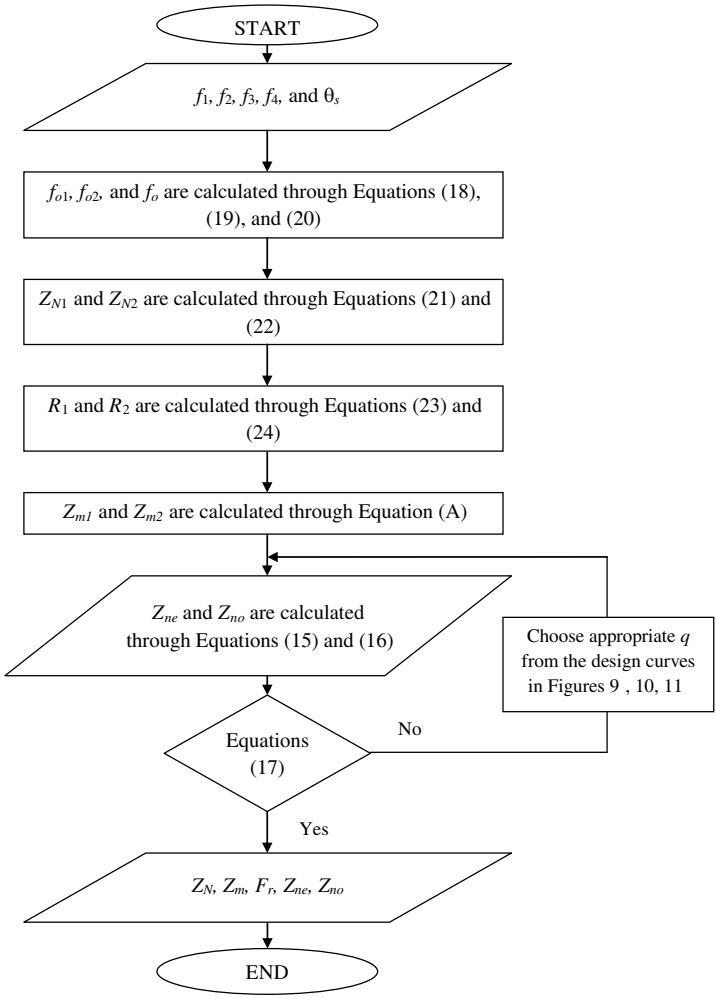

REFERENCES

1. Karthikeyan, S. S. and R. S. Kshetrimayum, "Compact, harmonic suppressed power divider using open complementary split-ring resonator," *Microwave and Optical Technology Letters*, Vol. 53, No. 12, 2897–2899, Dec. 2011.
2. Elez, A. V., P. V. Elez, J. Bonache, and F. Martin, "Compact power dividers with filtering capability for ground penetrating RADAR applications," *Microwave and Optical Technology Letters*, Vol. 54, No. 3, 608–611, Mar. 2012.
3. Mitu, S. S. I., S. L. Taiwo, and M. Sharawi, "Aperture stacked

microstrip equal/unequal power divider," *Microwave and Optical Technology Letters*, Vol. 54, No. 3, 784–785, Mar. 2012.

4. Ahmed, O. M. H., A. Elboushi, A.-R. Sebak, and T. A. Denidni, "Numerical and experimental investigations of defected ground triangular-shaped power divider for C-band applications," *Microwave and Optical Technology Letters*, Vol. 54, No. 4, 1022–1028, Apr. 2012.
5. He, J., Z. F. Chen, B. H. Yang, and M. Y. Xiong, "Miniaturized microstrip Wilkinson power divider with capacitor loading," *Microwave and Optical Technology Letters*, Vol. 54, No. 1, 61–63, Jan. 2012.
6. Zhou, B., W. Sheng, and H. Wang, "Harmonics suppression of Wilkinson power divider using bond wires with adjustable rejection bands," *Microwave and Optical Technology Letters*, Vol. 54, No. 3, 775–777, Mar. 2012.
7. Zhuge, C., K. Song, and Y. Fan, "Ultra-wideband (UWB) power divider based on signal interference techniques," Vol. 54, No. 4, 1028–1030, Apr. 2012.
8. Ibrahim, S. Z., M. E. Bialkowski, and A. M. Abbosh, "Ultra wideband quadrature power divider employing double wireless via," *Microwave and Optical Technology Letters*, Vol. 54, No. 2, 300–305, Feb. 2012.
9. Li, B., X. Wu, N. Yang, and W. Wu, "Dual-band equal/unequal Wilkinson power divider based on coupled-line section with short-circuited stub," *Progress In Electromagnetics Research*, Vol. 111, 163–178, 2011.
10. Shamaileh, K., A. Qaroot, and N. Dib, "Non-uniform transmission line transformers and their application in the design of compact multi-band power dividers," *Progress In Electromagnetics Research*, Vol. 113, 269–284, 2011.
11. Shamaileh, K., A. Qaroot, N. Dib, and A. Sheta, "Design and analysis of multi-frequency Wilkinson power dividers using non-unifor transmission lines," *International Journal of RF and Microwave Computer-aided Engineering*, Vol. 21, No. 5, 526–533, 2011.
12. Bao, X. L., G. Ruvio, and M. J. Ammann, "Directional dual-band slot antenna with dual bandgap high impedance surface reflector," *Progress In Electromagnetics Research C*, Vol. 9, 1–11, 2009.
13. Srisathit, S., S. Vimnphun, K. Bandudej, M. Chongcheawchanman, and A. Worapishet, "A dual-band 3-dB three-port power divider based on a two-section transmission line transformer," *IEEE MTT-S Int. Microwave Symposium Digest*, Vol. 1, 35–38, 2003.

14. Wu, L., Z. Sun, H. Yilmaz, and M. Berroth, "A dual-frequency Wilkinson power divider," *IEEE Transaction on Microwave Theory and Techniques*, Vol. 54, No. 1, 278–284, Jan. 2006.
15. Kampitaki, D. G., A. T. Hatzigaidas, A. I. Papastergiou, and Z. D. Zaharis, "On the design of a dual-band unequal power divider useful for mobile communications," *Electronic Engineering*, Vol. 89, 443–450, 2007.
16. Cheng, K. M. and C. Law, "A novel approach to the design and implementation of dual-band power divider," *IEEE Transaction on Microwave Theory and Techniques*, Vol. 56, No. 2, 487–491, Feb. 2008.
17. Monzon, C., "A small dual frequency transformer in two sections," *IEEE Trans. Microwave Theory and Technique*, Vol. 51, No. 4, 1157–1161, 2003.
18. Chongcheawchamnan, M., S. Patisang, S. Srisathit, R. Phromloungsri, and S. Bunnjwaht, "Analysis and design of three section transmission line transformer," *IEEE Transaction on Microwave Theory and Techniques*, Vol. 53, No. 7, 2458–2462, 2005.
19. Jwaied, H., F. Muwanes, and N. Dib, "Analysis and design of quad band four sections transmission line impedance transformer," *Aces Journal*, Vol. 22, 381–387, No. 3, 2007.
20. Dib, N. and M. Khodier, "Design and optimization of multi-band Wilkinson power divider," *International Journal of RF and Microwave-aided Engineering Wireless and Optical Communications*, 14–20, Sep. 2007.
21. Wang, X.-H., X. Chen, X.-W. Shi, F. Wei, and Y. Bai, "A novel planar three-way tri band power divider," *Microwave and Optical Technology Letters*, Vol. 52, No. 1, 182–184, Jan. 2010.
22. Jwaid, H., F. Muwanes, and N. Dib, "Design and analysis of quad-band Wilkinson power divider," *International Journal on Wireless and Optical Communications*, Vol. 4, No. 3, 305–312, 2007.
23. Mohra, A. S. and M. A. Alkanhal, "Dual band Wilkinson power divider using T-sections," *Journal of Microwave and Optoelectronics and Electromagnetic Applications*, Vol. 7, No. 2, 83–90, Dec. 2008.
24. Wu, Y., Y. Liu, and S. Li, "A compact pi-structure dual band transformer," *Progress In Electromagnetics Research*, Vol. 88, 121–134, 2008.
25. Jrad, A., T. Safarjalani, J.-M. Duchamp, P. Ferrari, and A. El-Helwani, "The three symmetric power divider ports, compact, fixed, and tunable based on microstrip technology," *Microwave*

and Optical Technology Letters, Vol. 51, No. 1, 229–232, Jan. 2009.

26. Wu, Y., Y. Liu, S. Li, and C. Yu, "Novel pi-type stepped-impedance stub branch line and its application to power divider with high suppression of intermediate frequencies," *Microwave and Optical Technology Letters*, Vol. 53, No. 10, 2360–2363, Oct. 2011.
27. Yang, T., C. Liu, L. Yan, and K. Huang, "A compact dual band power divider using planar artificial transmission lines For GSM/DCS applications," *Progress In Electromagnetics Research Letters*, Vol. 10, 185–191, 2009.
28. Chen, C.-C., H.-T. Sun, and Y.-R. Chen, "A novel unequal-power divider based on synthetic quasi-TEM transmission line design," *Microwave and Optical Technology Letters*, Vol. 54, No. 2, 535–539, Feb. 2012.
29. Russo, I., L. Boccia, G. Amendola, and H. Schumacher, "Compact hybrid coaxial architecture for UWB quasi-optical power combiners," *Progress In Electromagnetics Research*, Vol. 122, 77–92, 2012.
30. Wu, Y.-L., H. Zhou, Y.-X. Zhang, and Y.-A. Liu, "An unequal Wilkinson power divider for a frequency and its first harmonic," *IEEE Microwave and Wireless Components Letters,* Vol. 18, No. 11, 737–739, Nov. 2008.
31. Wu, Y., Y. Liu, and S. Li, "An unequal dual frequency Wilkinson power divider with optional isolation structure," *Progress In Electromagnetics Research*, Vol. 91, 393–411, 2009.
32. Wu, Y., Y. Liu, Y. Zhang, J. Gao, and H. Zhou, "A dual band unequal Wilkinson power divider without reactive components," *IEEE Transaction on Microwave Theory and Techniques*, Vol. 57, No. 1, 216–222, Jan. 2009.
33. Kim, T. G., B. Lee, and M.-J. Park, "Dual band unequal Wilkinson power divider with reduced length," *Microwave and Optical Technology Letters*, Vol. 52, No. 5, 1187–1190, May 2010.
34. Lin, Z. and Q.-X. Chu, "A novel approach to the design of dual-band power divider with variable power division ratio based on coupled lines," *Progress In Electromagnetics Research*, Vol. 103, 271–284, 2010.
35. Monjia, R., I. Bahl, and B. Bhartia, *RF and Microwave Coupled Line Circuits*, Artech House, 1999.
36. Matthaei, G. L., L. Young, and E. M. T. Jones, *Microwave Filters, Impedance-matching Networks, and Coupling Structures*, Chapter 7, 779, Artech House Inc., 1980.